Supplement of Atmos. Chem. Phys., 16, 277–292, 2016
http://www.atmos-chem-phys.net/16/277/2016/
doi:10.5194/acp-16-277-2016-supplement

Atmospheric Chemistry and Physics Open Access EGU

Supplement of

Plant surface reactions: an opportunistic ozone defence mechanism impacting atmospheric chemistry

W. Jud et al.

Correspondence to: A. Hansel (armin.hansel@uibk.ac.at)

1 The fate of the Criegee Intermediates

In our experiments we focused mainly on stable and volatile ozonolysis products, since these are the only ones directly accessible with SRI-ToF-MS. However, according to current understanding, there are many more possible ozonolysis products. Some of them are very short-lived, others too little volatile and therefore not measurable in the gas phase.

The Criegee mechanism (Criegee, 1975) predicts for gas phase ozone - alkene reactions a decomposition of the primary ozone-alkene addition product into a primary carbonyl compound and a highly excited Criegee Intermediate (CI). On the one hand, unimolecular reactions of unsubstituted (or monosubstituted) anti-CI conformers (terminal oxygen atom faces a hydrogen atom) are believed to yield excited organic acids, which might further dissociate to OH, H and organic radicals (Kroll et al., 2001). On the other hand, unimolecular reactions of disubstituted (or monosubstituted) syn-carbonyl oxides (terminal oxygen faces an alkyl group) are thought to form vinyl hydroperoxide intermediates (Kroll et al., 2001; Cremer, 1981), which will eventually decay forming OH radicals, too. In any case, the OH radicals formed in homogeneous ozone - alkene reactions play an important role in atmospheric chemistry, since their reaction rates with VOC are generally much higher than those of ozone (Atkinson and Arey, 2003). Atmospheric oxidation of VOC in regions with high NO_x concentrations leads again to the formation of ozone (Jenkin and Clemitshaw, 2000). The OH radical recycling is therefore crucial for the oxidizing capacity of the atmosphere.

However, in surface ozonolysis it can be assumed that the energy rich CI is efficiently relaxed through collisions at the surface, thus forming a Stabilized Criegee Intermediate (SCI). If this is the case, we would expect no OH formation from CI in the gas phase. In order to prove this hypothesis we've added cyclohexane as OH scavenger in some of our tobacco experiments. The results indeed indicate that no OH is released into or formed in the gas phase. Nonetheless, we cannot totally exclude OH formation from ozonolysis at the plant surface, where these radicals would be readily scavenged by reactive compounds (e.g. diterpenoids).

In the condensed phase additional reaction pathways for the SCI become available. First, it could undergo a 1,3-cycloaddition with the corresponding ozonolysis carbonyl in order to form a secondary ozonide (Criegee, 1975; Finlayson-Pitts and Pitts, 2000).

Secondly, different isomerisation reactions of the CI could result in stable products. The so-called hot organic acid from anti-CI might be collisionally stabilized at the surface. In the *cis*-abienol case one would expect formic acid from the CI formed in the ozonolysis of the terminal double bond. Formic acid is volatile enough and was detected by SRI-ToF-MS.

In the condensed phase the syn-CI could form a vinyl hydroperoxide which might isomerise to stable α-hydroxy ketones (Epstein and Donahue, 2008). Such molecules were found in ozonolysis experiments of skin oils containing squalene as major constituent (Wisthaler and Weschler, 2010). Indeed, we were able

to detect a compound at $m/z87.045$ ($C_4H_7O_2^+$) and $m/z116.035$ ($C_4H_6O_2 \bullet NO^+$) in H_3O^+ respectively NO^+ reagent ion mode, tentatively assigned to α-hydroxy-2-butenone. This compound could be formed along with MVK when the inner double bond of *cis*-abienol (see Fig. 1a) is attacked by ozone.
In the humid plant chamber environment (relative humidity ranged from about 55 % during dark conditions to > 80 % when plants were illuminated) reactions of the SCI in the liquid water layer at the plant surface could also form hydroxy-alkyl hydroperoxides. These could again decay forming carbonyls, acids, hydrogen peroxides, water and OH radicals, as known from gas phase reactions (Hasson et al., 2003).

2 Non-volatile ozonolysis carbonyls

As mentioned in the previous section, fragmentation of the ozone-alkene addition complex yields a carbonyl and a CI. In the case of *cis*-abienol ozonolysis, along with the volatile carbonyls MVK and formaldehyde also the corresponding longer chained carbonyls should be formed. These C_{16} respectively C_{19} compounds are expected to be non-volatile due to their estimated vapour pressure (Goldstein and Galbally, 2007) and will thus remain at the leaf surface. In order to test this, we stripped off the leaf surface compounds after the ozone fumigation experiments as described in the Materials and methods part. The samples were then analysed by GC-MS (see Materials and methods). However, lacking reference spectra of most of the expected non-volatile ozonolysis products, peak assignment was difficult. Nonetheless we could assign a peak with high certainty to sclaral, an isomerisation product of the C_{16} carbonyl from *cis*-abienol ozonolysis. Moreover we were able to detect large amounts of unreacted *cis*-abienol and CBTdiols in samples of the corresponding emitter plant.

3 Surface ozonolysis in tubing and at the plant enclosure surface

The diterpenoids released by the tobacco plants are semi- or low volatile. These terms usually refer to compounds having a low vapour pressure and high boiling point at room temperature (Goldstein and Galbally, 2007). Consequently, under standard conditions they remain mainly in the liquid or solid phase. This is for example the case for the diterpenoid *cis*-abienol, which is a solid at room temperature. Nonetheless, to some extent semi-volatile diterpenoids can evaporate into the gas phase and be deposited in places remote from their point of emission. Continuous condensation and evaporation of the semi-volatile compounds leads to an equilibrium between the gas and condensed phase.

In our experiments plants were installed in the plant enclosure the day before the actual measurement, so that they could adapt and recover from any stress experienced in the course of installation. During plant acclimation the plant enclosure was continuously flushed with clean, ozone free air. Since for example the semi-volatile *cis*-abienol (exuded by the *Ambalema* or *Basma Drama* trichomes) slowly evaporated into the gas phase, it covered over time - when ozone was not present - not only the plant surface, but

also the inner surface of the plant enclosure and the downstream tubing system. As a consequence, the *cis*-abienol covered surface area was increased. In the presence of ozone, the adsorbed *cis*-abienol at the enclosure and tubing surfaces was quickly depleted. This effect was responsible for bursts of the volatile diterpenoid oxidation products at the beginning of ozone fumigation (cf. Fig. 3). Eventually, a new equilibrium between diterpenoid production by the plant's trichomes and diterpenoid loss due to surface ozonolysis was established, along with a stable, positive carbonyl signal. Freshly deposited *cis*-abienol was then prevailingly covering the plant surface, which is closest to the trichomes.

To further investigate the impact of the surface ozonolysis in the tubing and at the enclosure surface, additional experiments with two plant enclosures in a row were conducted. To this end, the incoming air stream (see Materials and methods section) was split up in two parts. About $\sim 90\,\%$ of the flow was directed into the first plant enclosure containing a sample plant. The residual part ($\sim 10\,\%$) was directed through an ozone generator and could thereby be enriched with ozone. The air containing ozone could then be added either to the first plant enclosure or to the second, empty chamber. Fig. S1 shows the resulting MVK signal from *cis*-abienol ozonolysis in an experiment with an *Ambalema* plant. Ozone addition to the empty plant enclosure caused a short and less intense MVK burst deriving from surface ozonolysis of *cis*-abienol deposited during plant acclimation at the surface of the second chamber and tubing. After about 30 min (~ 3 gas exchange times of the chamber) the MVK signal became insignificant indicating that the surface deposited *cis*-abienol was consumed by ozonolysis and very few *cis*-abienol was resupplied by the air flow originating from the enclosure containing the sample plant. This implicates that gas phase reactions between *cis*-abienol and ozone are not relevant under fast gas exchange rates.
When in a second step the flow of ozonized air was directed to the first enclosure containing the sample plant, again a large burst of MVK from *cis*-abienol ozonolysis on all surfaces was observed. However, in contrast to the previous experiment, after a certain time span the MVK signal approximated a plateau well above the background level.

4 Relative humidity during ozone fumigation experiments

Several studies have reported on a humidity dependent ozone uptake of different plant types (see e.g. Lamaud et al., 2002; Altimir et al., 2004, 2006). Non-stomatal ozone deposition has been shown to increase significantly above a relative humidity (RH) of about 70 % (Lamaud et al., 2002; Altimir et al., 2006).
In our experiments the Ambalema variety showed a high total ozone conductance under dark conditions, which was about $4-5$ times higher than that of all other varieties. This cannot be explained by the RH alone. The relative humidities measured at the enclosure outlet were well below 70 % in all dark experiments, ranging from $\sim 54\,\%$ – $\sim 62\,\%$ (see Table S1). We conclude therefore that the RH had only

a minor impact on the total ozone conductance of the varieties tested.

5 2-day simulations of ozone protection through surface diterpenoids

In order to test the long term ozone protection efficiency of a leaf surface covered with diterpenoids, we conducted experiments lasting for two days (see Fig. S2). In the course of these experiments the ozone concentration in the plant enclosure was altered from 0-60 ppbv, mimicking diurnal ozone variations in the atmosphere. In experiments using *cis*-abienol emitters, the start of ozone fumigation led to the well-known rise of the corresponding oxidation products formaldehyde and MVK. Under light conditions and 20 ppbv ozone the *cis*-abienol signal dropped close to the detection limit. However, during the simulated night and without O_3 fumigation the signal recovered again to pre-fumigation levels. The second day of the experiments closely resembled the first day. Again, at certain ozone levels comparable amounts of oxidation products were formed, correlating with similar levels of overall ozone uptake in the plant enclosure. These results are strong indications that the diterpenoid layer at the surface of the emitting tobacco varieties provides long-term protection against ozone, highlighting its relevance.

6 Macroscopic model calculations

Similarly to the microscopic fluid dynamic simulations presented in the main text, we performed macroscopic model calculations (see Materials and methods). These show clearly the beneficial effect of ozone surface reactions. In Fig. S3 the ozone concentration isosurfaces are shown, where the ozone concentration is 10 % of the concentration in air entering the simulated box. For both the non-reactive (Fig. S3a) and the reactive plant (Fig. S3b), ozone uptake by the leaves under the given flow conditions results in an ozone depleted layer around the plant. Leaves located at the downwind side of the plant are generally exposed to less intense ozone stress. If the leaf surface is reactive (Fig. S3a), the ozone depleted layer is broader. When in real forest environments surface reactive plants grow close to each other, intrinsically unprotected plants growing in between benefit from the reduced ozone concentration, too. This effect could find application in agriculture similar to the push-pull concepts used against biotic stressors (Cook et al., 2007).

7 Comparison of stomatal ozone fluxes in the case of non-reactive and reactive leaf surfaces

In the case of a plant having a reactive leaf surface, the stomatal ozone flux is reduced compared to the same plant with an inert leaf surface. This can be shown mathematically. In the following calculations we use the same notation for ozone concentrations and resistances as in Fig. 5a+b in the main text.

In the case of a non-reactive (nr) leaf surface, the stomatal ozone flux $F_{\mathrm{s,nr}}$ equals the total ozone flux $F_{\mathrm{tot,nr}}$ entering the leaf boundary layer:

$$F_{\mathrm{s,nr}} = F_{\mathrm{tot,nr}} \tag{1}$$

Since ozone entering the stomata has to overcome the boundary layer resistance $R_{\mathrm{b,nr}}$ first, we can write:

$$F_{\mathrm{s,nr}} = \frac{c_{\mathrm{b,nr}} - c_{\mathrm{i}}}{R_{\mathrm{s}}} = \frac{c_{\mathrm{a}} - c_{\mathrm{b,nr}}}{R_{\mathrm{b,nr}}} \tag{2}$$

Assuming $c_{\mathrm{i}} = 0$ (Laisk et al., 1989) we get:

$$c_{\mathrm{b,nr}} = \frac{R_{\mathrm{s}} \cdot c_{\mathrm{a}}}{R_{\mathrm{s}} + R_{\mathrm{b,nr}}} \Longrightarrow \tag{3}$$

$$F_{\mathrm{s,nr}} = \frac{c_{\mathrm{a}}}{R_{\mathrm{s}} + R_{\mathrm{b,nr}}} \tag{4}$$

In the case of a reactive (r) leaf surface, due to the additional surface sink the total ozone flux $F_{\mathrm{tot,r}}$ is split into a stomatal flux $F_{\mathrm{s,r}}$ and a non-stomatal flux component $F_{\mathrm{ns,r}}$:

$$F_{\mathrm{tot,r}} = F_{\mathrm{s,r}} + F_{\mathrm{ns,r}} \tag{5}$$

Again, $F_{\mathrm{tot,r}}$ has to overcome the boundary layer resistance $R_{\mathrm{b,r}}$ and we can write:

$$\frac{c_{\mathrm{a}} - c_{\mathrm{b,r}}}{R_{\mathrm{b,r}}} = \frac{c_{\mathrm{b,r}} - c_{\mathrm{i}}}{R_{\mathrm{s}}} + \frac{c_{\mathrm{b,r}} - c_{\mathrm{c,r}}}{R_{\mathrm{sc}}} \tag{6}$$

Assuming again $c_{\mathrm{i}} = 0$ (Laisk et al., 1989) and $c_{\mathrm{c,r}} = 0$ in the case of a very reactive leaf surface with every ozone molecule lost at the surface we get:

$$\frac{c_{\mathrm{a}} - c_{\mathrm{b,r}}}{R_{\mathrm{b,r}}} = \frac{c_{\mathrm{b,r}}}{R_{\mathrm{s}}} + \frac{c_{\mathrm{b,r}}}{R_{\mathrm{sc}}} \Longrightarrow \tag{7}$$

$$c_{\mathrm{b,r}} = \frac{c_{\mathrm{a}} \cdot R_{\mathrm{s}} \cdot R_{\mathrm{sc}}}{R_{\mathrm{b,r}} \cdot (R_{\mathrm{s}} + R_{\mathrm{sc}}) + R_{\mathrm{s}} \cdot R_{\mathrm{sc}}} \Longrightarrow \tag{8}$$

$$F_{\mathrm{s,r}} = \frac{c_{\mathrm{a}} \cdot R_{\mathrm{sc}}}{R_{\mathrm{b,r}} \cdot (R_{\mathrm{s}} + R_{\mathrm{sc}}) + R_{\mathrm{s}} \cdot R_{\mathrm{sc}}} \tag{9}$$

Consequently, the fraction of the stomatal fluxes in the case of a reactive and a non reactive leaf surface is:

$$\frac{F_{\mathrm{s,r}}}{F_{\mathrm{s,nr}}} = \frac{\frac{c_{\mathrm{a}} \cdot R_{\mathrm{sc}}}{R_{\mathrm{b,r}} \cdot (R_{\mathrm{s}} + R_{\mathrm{sc}}) + R_{\mathrm{s}} \cdot R_{\mathrm{sc}}}}{\frac{c_{\mathrm{a}}}{R_{\mathrm{s}} + R_{\mathrm{b,nr}}}} \tag{10}$$

If we further assume that the boundary layer resistance does not change with the surface reactivity of a leaf ($R_{\mathrm{b,nr}} = R_{\mathrm{b,r}} =: R_{\mathrm{b}}$), we can simplify:

$$\frac{F_{\mathrm{s,r}}}{F_{\mathrm{s,nr}}} = \frac{R_{\mathrm{sc}} \cdot (R_{\mathrm{s}} + R_{\mathrm{b}})}{R_{\mathrm{b}} \cdot (R_{\mathrm{s}} + R_{\mathrm{sc}}) + R_{\mathrm{s}} \cdot R_{\mathrm{sc}}} \tag{11}$$

Eqn. 11 is graphically illustrated in Fig. S4, showing how $\frac{F_{\mathrm{s,r}}}{F_{\mathrm{s,nr}}}$ depends on different resistance ratios ($\frac{R_{\mathrm{s}}}{R_{\mathrm{sc}}}$ and $\frac{R_{\mathrm{s}}}{R_{\mathrm{b}}}$). In the case of $R_{\mathrm{sc}} \gg R_{\mathrm{s}}$, i.e. the leaf surface is inert, $\frac{F_{\mathrm{s,r}}}{F_{\mathrm{s,nr}}} \to 1$. In the case of a perfectly ozone scavenging leaf surface, $R_{\mathrm{sc}} \ll R_{\mathrm{s}}$ and $\frac{F_{\mathrm{s,r}}}{F_{\mathrm{s,nr}}} \to 0$, i.e. the stomatal flux $F_{\mathrm{s,r}}$ is much lower than $F_{\mathrm{s,nr}}$.

Strictly speaking, above calculations are correct only for perfectly inert or perfectly ozone scavenging leaf surfaces. In the case of a semi-reactive leaf surface, these calculations would be considerably more complicated, since in that case the ozone concentration within the leaf boundary layer is varying with the surface parallel distance from the stomata. Therefore different boundary layer concentrations have to be assumed as reference for stomatal and non-stomatal ozone fluxes to the leaf surface. In order to account for these varying boundary layer ozone concentrations, additional resistances have to be introduced (see next section).

8 Resistance scheme for ozone depletion on a semi-reactive leaf surface or in the case of non-zero intercellular ozone concentrations

In the main text we showed resistance schemes for ozone depletion on illuminated leaves having a non-reactive (Fig. 5a) and a reactive surface (Fig. 5b). In this respect, reactive means that every ozone molecule hitting the surface is being destroyed, resulting in an ozone concentration of zero at the leaf surface. In nature, however, the surface composition of leaves will always lie some point in between these two extremes: reactive semi-volatile compounds can be deposited on intrinsically non-reactive surfaces and not every ozone molecule hitting a semi-reactive (sr) surface will be destroyed. This situation can be depicted in a slightly more complex resistance scheme as shown in Fig. S5a. When the ozone depletion at the leaf surface is not complete, the ozone concentration in the leaf boundary layer is not equally distributed over the entire leaf surface. The ozone concentration is lowest close to the stomata ($c_{\mathrm{b,sr}}$) due

to the efficient stomatal sink. At a certain horizontal distance from the stomata, the ozone concentration in the leaf boundary layer ($c^*_{\mathrm{b,sr}}$) is higher if the surface is semi- or non-reactive. $c^*_{\mathrm{b,sr}}$ is the reference concentration for the surface chemical resistance $R_{\mathrm{sc,sr}}$.

The concentration gradient caused by the differences between $c_{\mathrm{b,sr}}$ and $c^*_{\mathrm{b,sr}}$ results in a diffusive ozone transport towards the stomatal pores. This fact is accounted for by introducing an additional resistance R_{x}, which limits this surface parallel transport path.

Conversely, in the case of non-zero intercellular ozone concentration (which has been observed e.g. in experiments applying extremely high ozone concentrations (> 1 *ppmv*, see Moldau and Bichele (2002)), but perfectly ozone scavenging leaf surface, the ozone concentration would be higher close the stomata and lower at a certain horizontal distance from the stomata. This would result in a diffusive ozone transport away from the stomata, thus eventually further limiting stomatal ozone uptake. In this case the same resistance scheme (Fig. S5a) could be used.

Applying now a Y-Δ transform (Kennelly, 1899), known from electrical circuits, we get the resistance scheme shown in Fig. S5b. Here, R'_{x}, R''_{x} and $R'_{\mathrm{b,sr}}$ can be obtained from R_{x}, $R_{\mathrm{b,sr}}$ and $R^*_{\mathrm{b,sr}}$.

The stomatal resistance R_{s} and R'_{x} as well as the surface chemical resistance $R_{\mathrm{sc,sr}}$ and R''_{x} could be combined to single resistances $R'_{\mathrm{s,sr}}$ ($= R_{\mathrm{s}} + R'_{\mathrm{x}}$) and $R'_{\mathrm{sc,sr}}$ ($= R_{\mathrm{sc,sr}} + R''_{\mathrm{x}}$), respectively. This implicates that the resistance scheme for a semi-reactive surface could be modelled similarly to that of a reactive leaf surface (see Fig. 5b). One should bear in mind though, that in this case $R'_{\mathrm{s,sr}}$ differs from R_{s} which is usually obtained from the stomatal conductance of water. To be precise, R'_{x} and R''_{x} have to be considered whenever there exists a surface parallel ozone gradient in the leaf boundary layer (cf. Fig. 5a), which is the case for semi- and non-reactive leaf surfaces (and stomata not being infinitely close to each other). R_{x} and therefore also R'_{x} and R''_{x} depend strongly on the sink strength of the leaf surface towards ozone. Only in the case of reactive leaf surfaces (cf. Fig. 5b+d) the net surface parallel ozone transport is zero and therefore $R'_{\mathrm{s,sr}} = R_{\mathrm{s}}$. While the range of R'_{x} and R''_{x} values is difficult to estimate, we want to point out here that disregarding $R_{\mathrm{sc,sr}}$ will lead to an overestimation of stomatal ozone flux, since $c_{\mathrm{b,sr}}$ strongly depends on the leaf surface sink.

References

Altimir, N., Tuovinen, J. P., Vesala, T., Kulmala, M., and Hari, P.: Measurements of ozone removal by Scots pine shoots: Calibration of a stomatal uptake model including the non-stomatal component, Atmospheric Environment, 38, 2387–2398, doi:10.1016/j.atmosenv.2003.09.077, 2004.

Altimir, N., Kolari, P., Tuovinen, J.-P., Vesala, T., Bäck, J., Suni, T., Kulmala, M., and Hari, P.: Foliage surface ozone deposition: a role for surface moisture?, Biogeosciences, 3, 209–228, doi:10.5194/bg-3-209-2006, 2006.

Atkinson, R. and Arey, J.: Atmospheric degradation of volatile organic compounds., Chemical Reviews, 103, 4605–4638, doi:10.1021/cr0206420, 2003.

Cook, S. M., Khan, Z. R., and Pickett, J. A.: The use of push-pull strategies in integrated pest management., Annual review of entomology, 52, 375–400, doi:10.1146/annurev.ento.52.110405.091407, 2007.

Cremer, D.: Theoretical determination of molecular structure and conformation. 7. Stereoselectivity of the ozonolysis reaction, Journal of the American Chemical Society, 103, 3619–3626, doi:10.1021/ja00403a001, 1981.

Criegee, R.: Mechanism of Ozonolysis, Angewandte Chemie International Edition in English, 14, 745–752, doi:10.1002/anie.197507451, 1975.

Epstein, S. A. and Donahue, N. M.: The kinetics of tetramethylethene ozonolysis: decomposition of the primary ozonide and subsequent product formation in the condensed phase., The journal of physical chemistry. A, 112, 13 535–13 541, doi:10.1021/jp807682y, 2008.

Finlayson-Pitts, B. J. and Pitts, J.: Chemistry of the Upper and Lower Atmosphere, Elsevier, San Diego, doi:10.1016/B978-012257060, 2000.

Goldstein, A. H. and Galbally, I. E.: Known and Unexplored Organic Constituents in the Earth's Atmosphere, Environmental Science & Technology, 41, 1514–1521, doi:10.1021/es072476p, 2007.

Hasson, A. S., Chung, M. Y., Kuwata, K. T., Converse, A. D., Krohn, D., and Paulson, S. E.: Reaction of Criegee Intermediates with Water Vapor - An Additional Source of OH Radicals in Alkene Ozonolysis?, The Journal of Physical Chemistry A, 107, 6176–6182, doi:10.1021/jp0346007, 2003.

Jenkin, M. E. and Clemitshaw, K. C.: Ozone and other secondary photochemical pollutants: chemical processes governing their formation in the planetary boundary layer, Atmospheric Environment, 34, 2499–2527, doi:10.1016/S1352-2310(99)00478-1, 2000.

Kennelly, A.: Equivalence of triangles and three-pointed stars in conducting networks, Electrical World and Engineer, 34, 413–414, 1899.

Kroll, J. H., Sahay, S. R., Anderson, J. G., Demerjian, K. L., and Donahue, N. M.: Mechanism of HO x Formation in the Gas-Phase Ozone-Alkene Reaction. 2. Prompt versus Thermal Dissociation of Carbonyl Oxides to Form OH, The Journal of Physical Chemistry A, 105, 4446–4457, doi:10.1021/jp004136v, 2001.

Laisk, A., Kull, O., and Moldau, H.: Ozone Concentration in Leaf Intercellular Air Spaces Is Close to Zero, Plant Physiology, 90, 1163–1167, doi:10.1104/pp.90.3.1163, 1989.

Lamaud, E., Carrara, A., Brunet, Y., Lopez, A., and Druilhet, A.: Ozone fluxes above and within a pine forest canopy in dry and wet conditions, Atmospheric Environment, 36, 77–88, doi:10.1016/S1352-2310(01)00468-X, 2002.

Moldau, H. and Bichele, I.: Plasmalemma protection by the apoplast as assessed from above-zero ozone concentrations in leaf intercellular air spaces, Planta, 214, 484–487, doi:10.1007/s00425-001-0678-0, 2002.

Wisthaler, A. and Weschler, C. J.: Reactions of ozone with human skin lipids: sources of carbonyls, dicarbonyls, and hydroxycarbonyls in indoor air., Proceedings of the National Academy of Sciences of the United States of America, 107, 6568–75, doi:10.1073/pnas.0904498106, 2010.

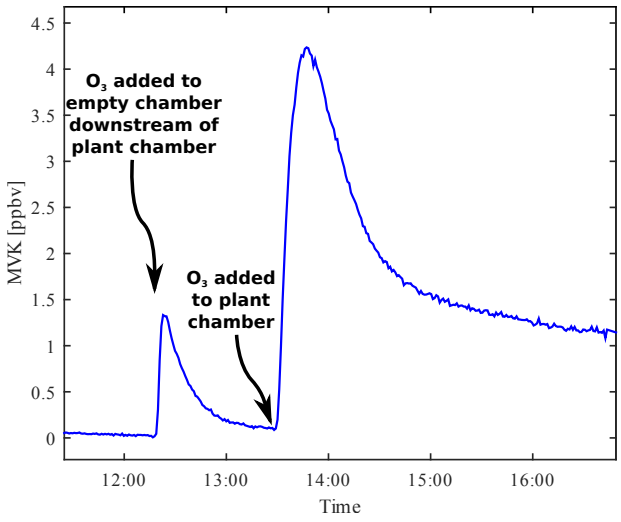

Figure S1: Two chamber ozone fumigation experiment with an *Ambalema* variety. The tobacco plant was installed in a plant enclosure, which was connected to a second, empty chamber at the downstream side. When ozone was added to the empty chamber, the MVK signal deriving from surface ozonolysis of semi-volatile *cis*-abienol deposited in the empty chamber decreased quickly. When ozone was added to the plant chamber, the MVK signal approximated a steady state, since the plant surface represented a continuous diterpenoid source. In this steady state, *cis*-abienol ozonolysis occurred prevailingly at the plant surface. For details refer to the text.

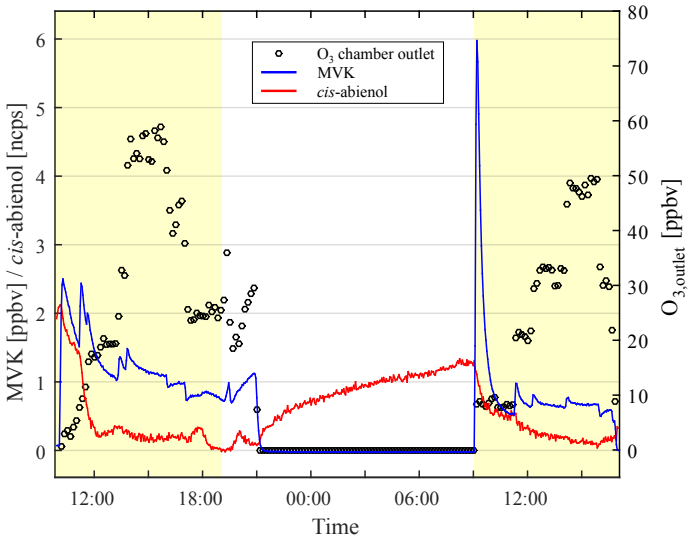

Figure S2: Experiment with an *Ambalema* plant simulating diurnal ozone variations. Yellow shaded areas represent times when the plant was illuminated. Addition of ozone resulted in an immediate reduction of the signal of semi-volatile *cis*-abienol and an initial MVK burst, deriving from *cis*-abienol ozonolysis on all surfaces. The *cis*-abienol signal recovered over night, leading to a huge MVK burst from surface ozonolysis at 09:00AM after restarting the ozone fumigation. Depicted ozone levels were measured at the plant enclosure outlet and are proportional to the total ozone flux.

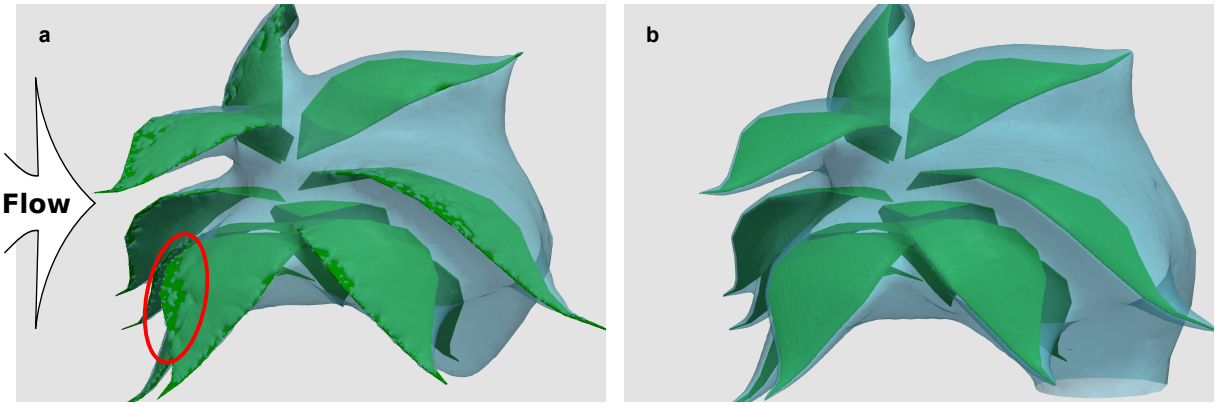

Figure S3: Macroscopic fluid dynamic calculations. The plots show the isosurfaces (in light blue color) of equal ozone concentration obtained from model simulations, in which similar plants without (**a**) or with (**b**) ozone-reactive leaf surface were fumigated with ozonated air (entering from the left side). The concentration at the isosurfaces corresponds to 10 % of the ozone concentration in the advecting air. In the case of a non-reactive leaf surface (**a**), solely stomatal uptake is responsible for the reduced ozone concentration in the leaf boundary layer. In places directly exposed to the advecting ozone-rich air, the leaf surface itself is exposed to high ozone concentrations (above the 10 % limit, see e.g. the area indicated by the red ellipse). In contrast, ozonolysis at the plant surface further reduces the ozone concentration in the air layer adjacent to the leaf surface (**b**). As a result, the reactive leaf surface expands the ozone depleted area. This effect, in combination with the lack of the pore effect for ozone on reactive leaf surfaces, diminishes the amount of phytotoxic ozone entering the leaf stomata.

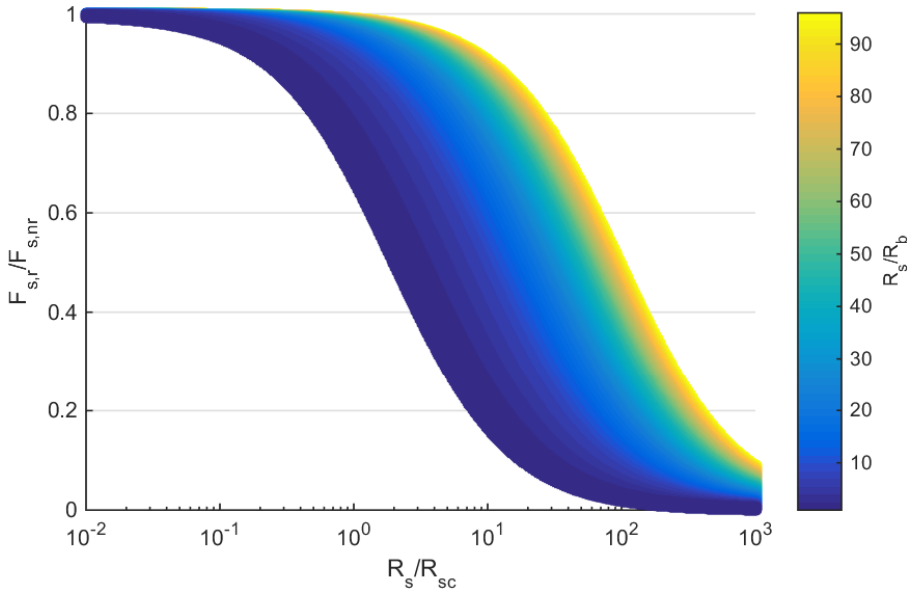

Figure S4: Comparison of stomatal ozone fluxes in the case of a non-reactive leaf surface ($F_{\mathrm{s,nr}}$) and a reactive leaf surface ($F_{\mathrm{s,r}}$). The stomatal ozone flux varies depending on the surface reactivity, which is inversely proportional to the surface chemical resistance R_{sc}. Moreover, also the boundary layer resistance R_{b} influences the stomatal flux.

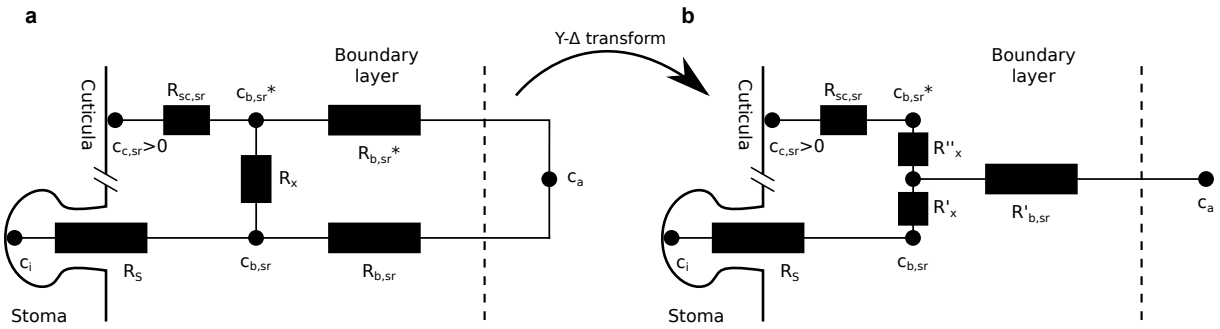

Figure S5: Resistance scheme of ozone uptake by a plant leaf with a semi-reactive (sr) surface or in the case of non-zero intercellular ozone concentrations (c_i). c_c, c_b and c_a denote ozone concentrations at the leaf surface, in the boundary layer and in ambient air, respectively. R_s, R_sc and R_b denote the stomatal, surface chemical and boundary layer resistances. R_x limits the surface parallel ozone transport in the leaf boundary layer from the cuticula towards the stomatal pores. The resistance scheme in **a** can be transformed into that shown in **b** by applying a Y-Δ transform. For details refer to the text.

Table S1: Relative humidities *RH* in the plant enclosure during ozone fumigation experiments of different tobacco varieties. Values are given for the same time ranges, for which the total ozone conductance has been calculated (see Fig. 4) and include standard errors of 5 (13), 2 (6), 1 (5) and 3 (5) replicates of *Ambalema*, *Basma Drama*, *BYBA* respectively *3H02* in dark (light) experiments.

	RH [%]	
Plant variety	dark	light
Ambalema	62 ± 2	78 ± 2
Basma Drama	55 ± 2	79 ± 4
BYBA	60	86 ± 1
3H02	54 ± 2	76 ± 2